Received: 8 October 2022 | Accepted: 15 December 2022

DOI: 10.1002/pamm.202200233

Geometric and material sensitivities for elasto-plasticity including non-local damage regularisation

Fabian Guhr[1,*] and **Franz-Joseph Barthold**[1]

[1] Structural Mechanics, TU Dortmund University, August-Schmidt-Str. 8, D-44227 Dortmund, Germany

Sensitivity analysis is applied to a regularised non-local ductile damage model. A variational approach is utilised to derive the analytical gradients of different objectives with respect to either geometrical of material parameters. Due to the definition of the material model, enhanced algorithmic treatments are necessary to capture its history dependent nature within the sensitivity computation. The gradient information with respect to the geometrical parameters are used to derive damage tolerant geometries in shape optimisation using Sequential Quadratic Programming (SQP). The sensitivities with respect to the material parameters are used to analyse the response and impact of certain material parameters of the model during loading and unloading of a specimen.

1 Introduction

For accurate simulation and optimisation of processes, accurate models for the underlying material behaviour are required. For metals in general, plastic behaviour should be included. Those plastic effects are already a well-known and established field in material modelling. Enhancing this behaviour by adding damaging effects leads to ductile damaging material models and are of great interest but introduce challenging problems to be solved.

The main problem is the underlying mesh-dependence of well-established damage models. One approach to circumvent this problem is the application of the so-called micro-morphic approach, wherein a non-local field variable is coupled to the local evolving damage by means of a penalty approach. Subsequently, the non-local variable is regularised on the global scale. Such a model is described in [1] and circumvents solving the Karush-Kuhn-Tucker conditions on the global scale, see e.g. [2] or [3] where this is required.

Utilising a variational approach to derive the sensitivities for the above model allows for an efficient way of obtaining the analytical gradients for shape optimisation and material sensitivity studies. The direct approach is applied which integrates nicely into the iterative solution scheme of elasto-plastic damage. Furthermore, the chosen optimisation problem contains many constraints which is beneficial for the direct method. With this approach, the gradients can be derived before applying the finite element discretisation. Due to the definition of the material model and utilisation of state-dependent history variables, those need to be taken into account when calculating the derivatives. This in return requires the adaptation of the general optimisation framework to update certain matrices throughout the optimisation process to accurately calculate the gradients.

2 Structural and sensitivity analysis

2.1 Material model

The material model used in this work has been derived in [1]. Therein, an elasto-plastic material model is regularised by a micro-morphic approach. With this concept, a local damage variable d is coupled to a non-local field variable ϕ by means of a penalty approach and subsequently regularised by a gradient-enhancement of the non-local damage variable. The non-local free energy thusly reads

$$\Psi^{\mathrm{nl}} = \frac{c_{\mathrm{d}}}{2} \|\nabla_{\boldsymbol{X}} \phi\|^2 + \frac{\beta_{\mathrm{d}}}{2} \left[\phi - d\right]^2 , \tag{1}$$

with the regularisation parameter c_{d} and the penalty parameter β_{d}. Combination of this non-local term with a standard local term defines the postulated total free energy

$$\Psi = \Psi^{\mathrm{loc}}(\boldsymbol{F}, \boldsymbol{h}^{\mathrm{p}}, d) + \Psi^{\mathrm{nl}}(\boldsymbol{F}, \boldsymbol{h}^{\mathrm{p}}, d, \phi, \nabla_{\boldsymbol{X}} \phi). \tag{2}$$

Herein, $\boldsymbol{F}$ is the deformation gradient and $\boldsymbol{h}^{\mathrm{p}}$ captures all necessary history variables which are associated with plasticity. The above local energy term can theoretically be of any local type and is independent of the choice for the non-local quantity. This type of approach has the advantage that the resulting Karush-Kuhn-Tucker equations only have to be solved on the local level.

* Corresponding author: e-mail fabian.guhr@tu-dortmund.de, phone +49 231 755 7244, fax +49 231 755 7260

Subsequent integration over the volume $\mathcal{B}_0$ and surface $\partial\mathcal{B}_0$ of the undeformed body, as well as the postulate of minimum potential energy leads to the weak form as

$$r^{\varphi} = \int_{\mathcal{B}_0} \frac{\partial \Psi}{\partial \boldsymbol{F}} : \nabla_{\boldsymbol{X}} \boldsymbol{\eta}^{\varphi} - \boldsymbol{B} \cdot \boldsymbol{\eta}^{\varphi} \, \mathrm{d}V - \int_{\partial\mathcal{B}_0} \boldsymbol{T} \cdot \boldsymbol{\eta}^{\varphi} \, \mathrm{d}A = 0, \tag{3}$$

$$r^{\phi} = \int_{\mathcal{B}_0} \frac{\partial \Psi}{\partial \nabla_{\boldsymbol{X}} \phi} \cdot \nabla_{\boldsymbol{X}} \eta^{\phi} + \frac{\partial \Psi}{\partial \phi} \eta^{\phi}] \, \mathrm{d}V = 0. \tag{4}$$

Herein, $\boldsymbol{\eta}^{\varphi}$ represents the deformation test function, while η^{ϕ} represents the damage test function. The occurring derivatives can be identified as the first Piola-Kirchhoff stress tensor $\boldsymbol{P}$, as well as the non-local damage driving forces $\boldsymbol{Y}$ and Y, i.e.

$$\boldsymbol{P} := \frac{\partial \Psi}{\partial \boldsymbol{F}}, \qquad \boldsymbol{Y} := \frac{\partial \Psi}{\partial \nabla_{\boldsymbol{X}} \phi}, \qquad Y := \frac{\partial \Psi}{\partial \phi}. \tag{5}$$

Combining both residuals leads to the total residual form

$$\boldsymbol{R} = \begin{bmatrix} r^{\varphi} \\ r^{\phi} \end{bmatrix} = \boldsymbol{0}. \tag{6}$$

Applying a standard finite element discretisation and an isoparametric concept for the shapes functions, as well as utilising the Bubnov-Galerkin-method, allows the finite element formulation for the above residual. Subsequent linearisation for the global Newton-iteration leads to

$$\begin{bmatrix} \mathbf{r}^{\varphi} \\ \mathbf{r}^{\phi} \end{bmatrix} = \begin{bmatrix} \mathbf{K}^{\varphi\varphi} \mathbf{K}^{\varphi\phi} \\ \mathbf{K}^{\phi\varphi} \mathbf{K}^{\phi\phi} \end{bmatrix} \cdot \begin{bmatrix} \Delta\boldsymbol{\varphi} \\ \Delta\boldsymbol{\phi} \end{bmatrix} = \mathbf{r} + \mathbf{K} \cdot \Delta\mathbf{w} = \mathbf{0}. \tag{7}$$

Additional information regarding implementation, the local model and all further necessary terms and aspects can be taken from the original source [1].

2.2 Sensitivity analysis

The ansatz for deriving the sensitivities of the above model is that, for an arbitrarily chosen design $\boldsymbol{s}$ the equilibrium condition in (6) has to always be fulfilled, hence its total variation has to vanish, cf. [3, 5, 7]. For the underlying model this leads to the partial variations

$$\delta\boldsymbol{R} = \delta_{\boldsymbol{w}}\boldsymbol{R} + \delta_{\boldsymbol{s}}\boldsymbol{R} + \delta_{\boldsymbol{h}_n}\boldsymbol{R} = \boldsymbol{k}(\boldsymbol{\eta}, \delta\boldsymbol{w}) + \boldsymbol{p}(\boldsymbol{\eta}, \delta\boldsymbol{s}) + \boldsymbol{h}(\boldsymbol{\eta}, \delta\boldsymbol{h}_n) = \boldsymbol{0}. \tag{8}$$

Therein, the partial variation with respect to the field variables can be identified as the tangent stiffness $\boldsymbol{k}$. The new additional terms denote the pseudo load $\boldsymbol{p}$ and the history sensitivity $\boldsymbol{h}$. The pseudo load term is the partial variation of the residual with respect to the design and consists of the deformation part

$$p^{\varphi} = \delta_{\boldsymbol{s}} r^{\varphi} = \int_{\mathcal{B}_\zeta} \delta_{\boldsymbol{s}}\boldsymbol{P} : \nabla_{\boldsymbol{X}} \boldsymbol{\eta}^{\varphi} J_K \, \mathrm{d}V_\zeta + \int_{\mathcal{B}_\zeta} \boldsymbol{P} : \delta_{\boldsymbol{s}} \nabla_{\boldsymbol{X}} \boldsymbol{\eta}^{\varphi} J_K \, \mathrm{d}V_\zeta + \int_{\mathcal{B}_\zeta} \boldsymbol{P} : \nabla_{\boldsymbol{X}} \boldsymbol{\eta}^{\varphi} \, \delta_{\boldsymbol{s}} J_K \, \mathrm{d}V_\zeta \tag{9}$$

and the damage part

$$p^{\phi} = \delta_{\boldsymbol{s}} r^{\phi} = \int_{\mathcal{B}_\zeta} \left[\delta_{\boldsymbol{s}} Y \, \eta^{\phi} + \delta_{\boldsymbol{s}} \boldsymbol{Y} \cdot \nabla_{\boldsymbol{X}} \eta^{\phi} + \boldsymbol{Y} \cdot \delta_{\boldsymbol{s}} \nabla_{\boldsymbol{X}} \eta^{\phi} \right] J_K \, \mathrm{d}V_\zeta + \int_{\mathcal{B}_\zeta} \left[\boldsymbol{Y} \cdot \nabla_{\boldsymbol{X}} \eta^{\phi} + Y \, \eta^{\phi} \right] \delta_{\boldsymbol{s}} J_K \, \mathrm{d}V_\zeta. \tag{10}$$

These quantities are based on utilising the enhanced kinematic framework, c.f. [3, 5–8]. Application of the framework allows for an easy approach to derive the variations with respect to the geometry $\boldsymbol{X}$ by introduction of a parameter space, which allows the decoupling of the implicit dependencies of geometry and deformation. As such, by choosing the design to be equal to the geometry, i.e. $\boldsymbol{s} = \boldsymbol{X}$, the above integrals take the forms

$$\begin{aligned} p^{\varphi}_{\boldsymbol{X}} = & \int_{\mathcal{B}_\zeta} \nabla_{\boldsymbol{X}} \boldsymbol{\eta}^{\varphi} : \frac{\mathrm{d}\boldsymbol{P}}{\mathrm{d}\boldsymbol{F}} : \delta_{\boldsymbol{X}} \boldsymbol{F} J_K \, \mathrm{d}V_\zeta \\ & - \int_{\mathcal{B}_\zeta} \boldsymbol{P} : \left[\nabla_{\boldsymbol{X}} \boldsymbol{\eta}^{\varphi} \cdot \nabla_{\boldsymbol{X}} \delta\boldsymbol{X} \right] J_K \, \mathrm{d}V_\zeta + \int_{\mathcal{B}_\zeta} \boldsymbol{P} : \nabla_{\boldsymbol{X}} \boldsymbol{\eta}^{\varphi} \, \left[\nabla_{\boldsymbol{X}} \cdot \delta\boldsymbol{X} \right] J_K \, \mathrm{d}V_\zeta \end{aligned} \tag{11}$$

for the deformation part and

$$p^{\phi}_{\boldsymbol{X}} = \int_{\mathcal{B}_\zeta} \left[\frac{\mathrm{d}Y}{\mathrm{d}\boldsymbol{F}} : \delta_{\boldsymbol{X}} \boldsymbol{F}\, \eta^{\phi} - \nabla_{\boldsymbol{X}} \eta^{\phi} \cdot [\boldsymbol{Y} \cdot \nabla_{\boldsymbol{X}} \delta \boldsymbol{X}] - \boldsymbol{Y} \cdot \left[\nabla_{\boldsymbol{X}} \eta^{\phi} \cdot \nabla_{\boldsymbol{X}} \delta \boldsymbol{X} \right] \right] J_K \, \mathrm{d}V_\zeta + \int_{\mathcal{B}_\zeta} \left[\boldsymbol{Y} \cdot \nabla_{\boldsymbol{X}} \eta^{\phi} + Y\, \eta^{\phi} \right] J_K \nabla_{\boldsymbol{X}} \cdot \delta \boldsymbol{X} \, \mathrm{d}V_\zeta \tag{12}$$

for the damage part. While in the above equations the geometry $\boldsymbol{X}$ is defined as the design, in the actual application the geometry is coupled to control points $\boldsymbol{p}$ of a chosen Computer Aided Geometric Design (CAGD). Hence, a so-called design velocity matrix $\mathbf{Q}$ is introduced to couple the finite element geometry $\boldsymbol{X}$ to the actual design variables $\boldsymbol{p}$, i.e.

$$\delta \boldsymbol{X} = \frac{\partial \boldsymbol{X}}{\partial \boldsymbol{p}} \delta \boldsymbol{p} = \mathbf{Q}\, \delta \boldsymbol{p}. \tag{13}$$

Choosing the material parameters as the design, i.e. $\boldsymbol{s} = \boldsymbol{m}_p$, leads to the following more straightforward pseudo load terms, since the geometric description is independent of the material parameter. As such, the variations of the gradients of shape function, as well as of the mapping vanish, leaving only the variational terms of the driving forces. The integrals read

$$p^{\varphi}_{\boldsymbol{m}} = \int_{\mathcal{B}_0} \nabla_{\boldsymbol{X}} \boldsymbol{\eta}^{\varphi} : \frac{\mathrm{d}\boldsymbol{P}}{\mathrm{d}\boldsymbol{m}_p} \, \mathrm{d}V \quad \text{and} \quad p^{\phi}_{\boldsymbol{m}} = \int_{\mathcal{B}_0} \eta^{\phi} \frac{\mathrm{d}Y}{\mathrm{d}\boldsymbol{m}_p} + \nabla_{\boldsymbol{X}} \eta^{\phi} \cdot \frac{\mathrm{d}\boldsymbol{Y}}{\mathrm{d}\boldsymbol{m}_p} \, \mathrm{d}V \tag{14}$$

for the respective deformation and damage part.

The history sensitivity $\boldsymbol{h}$ in Eq. (8) is split into two parts as well, i.e.

$$h^{\varphi} = \delta_{\boldsymbol{h}_n} r^{\varphi} = \int_{\mathcal{B}_\zeta} \delta_{\boldsymbol{h}_n} \boldsymbol{P} : \nabla_{\boldsymbol{X}} \eta^{\varphi} \, J_K \, \mathrm{d}V_\zeta \quad \text{and} \quad h^{\phi} = \delta_{\boldsymbol{h}_n} r^{\phi} = \int_{\mathcal{B}_\zeta} \delta_{\boldsymbol{h}_n} Y \eta^{\phi} J_K \, \mathrm{d}V_\zeta \tag{15}$$

for the respective deformation and damage part, where the partial variation of the tensorial non-local damage driving force vanishes, since $\boldsymbol{Y}$ is independent of the internal history variables.

Due to the history dependent structure, i.e. the internal history variables $\boldsymbol{h} = \left\{ \boldsymbol{C}^{\mathrm{p}-1}, \alpha, d \right\}$ evolve at each load step, the total variation of the history variables have to be computed after each converged global Newton-iteration of the structural analysis. These are important to derive the sensitivity matrix $\mathbf{S}$ in Eq. (18) to couple the history variables to the design variables. The total variation of the history variables reads

$$\delta \boldsymbol{h} = \delta_{\boldsymbol{w}} \boldsymbol{h} + \delta_{\boldsymbol{s}} \boldsymbol{h} + \delta_{\boldsymbol{h}_n} \boldsymbol{h}. \tag{16}$$

The choice of design variables, i.e. $\boldsymbol{s} = \boldsymbol{X}$ or $\boldsymbol{s} = \boldsymbol{m}_p$, also applies to the computation of the total variation of the history variables.

Applying the same finite element discretisation as exercised for the structural analysis problem in the previous section, the total variation in Eq. (8) takes the matrix form

$$\delta \mathbf{R} = \mathbf{K}\, \delta \mathbf{w} + \mathbf{P}\, \delta \mathbf{s} + \mathbf{H}\, \delta \mathbf{h}_n = \mathbf{0}, \tag{17}$$

with the stiffness matrix $\mathbf{K} \in \mathbb{R}^{\mathrm{ndof} \times \mathrm{ndof}}$, the pseudo load matrix $\mathbf{P} \in \mathbb{R}^{\mathrm{ndof} \times \mathrm{ndv}}$ and the history sensitivity matrix $\mathbf{H} \in \mathbb{R}^{\mathrm{ndof} \times \mathrm{nhv}}$. The quantities for the dimensions represent the number of degrees of freedom ndof, which is equal to the number of element nodes times the number of dimensions ndim plus one, to also capture the nodal damage values. ndv is the number of design variables, which in this work either is equal to the number of control points $\mathbf{p}$ of the geometric shape or the number of material parameters $\mathbf{m}$, which for the underlying model is equal to 15, cf. [1] for a detailed analysis of the impact of each parameter and in Sec. 3.2 below. Finally, nhv captures the number of history variables which for the sake of implementation is equal to 11 at each local Gauss-point.

Reordering of Eq. (17) allows the computation of the sensitivity matrix $\mathbf{S}$, i.e.

$$\delta \mathbf{w} = -\mathbf{K}^{-1} \left[\mathbf{P}\, \delta \mathbf{s} + \mathbf{H}\, \delta \mathbf{h}_n \right] = -\mathbf{K}^{-1} \left[\mathbf{P} + \mathbf{H} \mathbf{Z}_n \right] \delta \mathbf{s} = \mathbf{S}\, \delta \mathbf{s}. \tag{18}$$

The sensitivity matrix $\mathbf{S} \in \mathbb{R}^{\mathrm{ndof} \times \mathrm{ndv}}$ describes the response of the field variables of the structural analysis $\mathbf{w}$ due to a change in design $\mathbf{s}$ and is required for the computation of additional gradients for the objective functions and constraints for subsequent optimisation problems. The new matrix $\mathbf{Z}$ is updated after calculation of the sensitivity matrix $\mathbf{S}_{n+1}$ for each load step n and subsequently generated by substituting the total variation of the history variables from the previous load step, i.e.

$$\delta \mathbf{h}_{n+1} = \left[\frac{\mathrm{d}\mathbf{h}}{\mathrm{d}\mathbf{w}} \mathbf{S} + \frac{\mathrm{d}\mathbf{h}}{\mathrm{d}\mathbf{s}} + \frac{\mathrm{d}\mathbf{h}}{\mathrm{d}\mathbf{h}_n} \mathbf{Z}_n \right] \delta \mathbf{s} = \mathbf{Z}_{\mathrm{n}+1}\, \delta \mathbf{s}, \tag{19}$$

which again highlights the importance of updating the total variation of the history variable at each converged global Newton-iteration, since these information are required to derive the sensitivity matrix in the next load step. At the beginning of the simulation $t = t_0$ the initial total variation of the history variable is assumed to be zero, i.e. $\delta \mathbf{h}_0 = \mathbf{0}$, leading to

$$\mathbf{S}_1 = -\mathbf{K}^{-1} \mathbf{P} \quad \text{with} \quad \mathbf{Z}_0 = \mathbf{0}. \tag{20}$$

3 Results

3.1 Shape optimisation

The aim of the shape optimisation is to generate shapes which are more damage resistant. For this example, taken from [4] and elaborated in more detail, is a plate with a hole problem and chosen for its inhomogeneous deformation and stress state. The plate is meshed with 1350 elements and the shape functions are of linear type for the approximation of deformation and global damage. Furthermore, for an enhanced regularisation behaviour, the $\bar{\boldsymbol{F}}$-method is applied, c.f. [9]. The number of elements combined with the $\bar{\boldsymbol{F}}$-method show a sufficient regularisation behaviour regarding the damage evolution, while simultaneously allowing for adequately low computational effort. As the design variables for the optimisation, the control points of a CAGD are chosen. These require additional equality constraints to generate a smooth geometry, which are straight forward and not specified here. To solve the optimisation problem, Sequential Quadratic Programming is utilised.

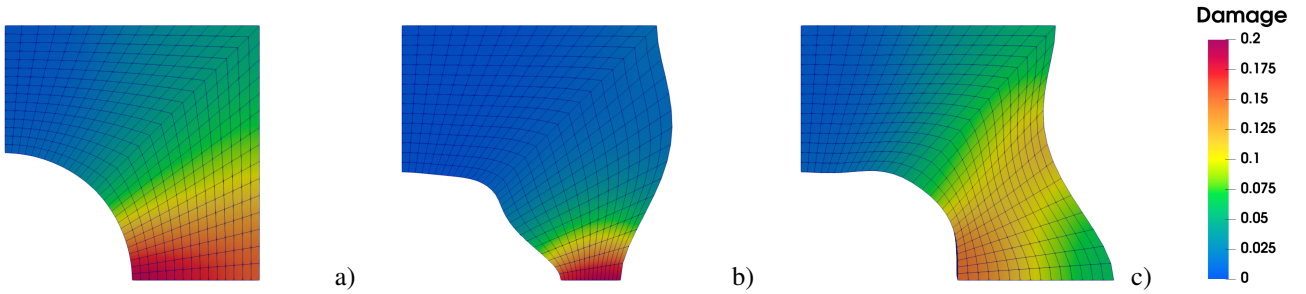

Fig. 1: The three shapes for the damage optimisation. Shape (a) depicts the referential design and damage distribution. In (b) the results of the first damage optimisation problem without damage constraints is depicted. (c) shows the final design where additionally nodal damage constraints are applied to the damage minimisation.

To reduce the damage accumulation, an immediate ansatz is to simply minimise the accumulated damage within a given body. This can be captured by a least-square function of all nodal damage values. An additional volume constraint is applied such that the total material in the body is simply reordered without adding or subtracting material to the body under consideration. The initial optimisation problem thus reads

$$\begin{aligned} \underset{\boldsymbol{s}_l \leq \boldsymbol{s} \leq \boldsymbol{s}_u}{\text{minimise}} \quad & \mathfrak{J}_1 = \|\boldsymbol{\phi}(\boldsymbol{s})\|^2 \\ \text{subject to} \quad & V(\boldsymbol{s}) = V_0. \end{aligned} \tag{21}$$

The solution to this optimisation problem is depicted in Fig. 1b. The optimal solution generated by minimisation of the problem in (21) leads to a decrease in cross section area in the lower part of the plate, which in return leads to rapid localisation of damage during loading and with that a reduction in stiffness. Furthermore, the maximum damage value in this cross-section of $\phi^1_{\max} = 0.1930$ also exceeds the initial value $\phi^0_{\max} = 0.1893$. As such, the simple minimisation of overall damage accumulation leads to a minimisation induced early localisation of damage in the critical area of the specimen. This is also detectable in the respective force-displacement curve, Fig. 2a. Due to the early localisation of damage, the reaction forces drastically drop, compared to the original shape.

This initial result is not the desired outcome of such an optimisation problem. A more desired outcome for such an optimisation problem would be a reordering of the material such that the damage is distributed more evenly, preventing possible failure due to reaching a critical damage threshold. This could in return circumvent early localisation when further loading is applied. To capture this in the optimisation, a second optimisation problem is proposed, wherein additional constraints for the maximum damage value of each nodal damage variable is added, i.e.

$$\begin{aligned} \underset{\boldsymbol{s}_l \leq \boldsymbol{s} \leq \boldsymbol{s}_u}{\text{minimise}} \quad & \mathfrak{J}_2 = \|\boldsymbol{\phi}(\boldsymbol{s})\|^2 \\ \text{subject to} \quad & V(\boldsymbol{s}) = V_0 \\ & \phi_i(\boldsymbol{s}) \leq \phi_{\text{crit}}. \end{aligned} \tag{22}$$

As such, this optimisation directly constraints the solution generated in (21) for a sufficiently small chosen value for ϕ_{crit}. The choice of ϕ_{crit} can be arbitrary, e.g. the initial maximum damage value $\phi_{\text{crit}} = \phi^0_{\max} = 0.1893$, but it is chosen as $\phi_{\text{crit}} = 0.15$. This can be imagined to be chosen, such that an arbitrary critical damage value is not exceeded, which in reality could result in failure of the underlying specimen.

The result of the optimisation is depicted in Fig. 1c. The optimisation problem leads to a shape, which more evenly distributes the accumulated damage throughout the body. This is accomplished by shifting the lower cross-section to the right, while simultaneously slightly increasing this area. Furthermore, a curvature is induced into the right edge of the specimen. As expected, the value of the objective function for this problem ($\mathfrak{J}_2 = 11.6341$) is larger than the unconstrained value

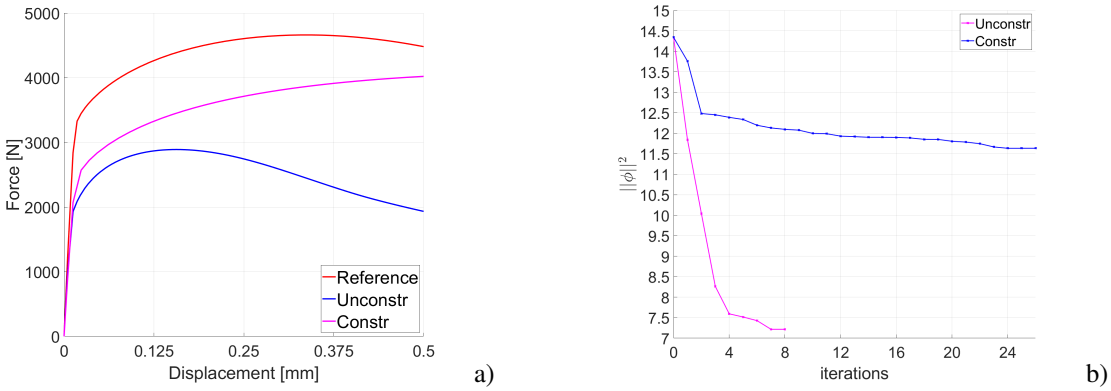

Fig. 2: The left graphs shows the structural response of the different designs with the reference design (red), the unconstrained optimisation problem 1 (blue) and the constrained optimisation problem 2 (magenta). The right graphs depicts the values of the chosen objective function of the number of iterations.

($\mathfrak{J}_1 = 7.2174$), see Fig. 2b. Still, even with the additional constraints, the overall accumulated damage in the generated structure is smaller than the initial value ($\mathfrak{J}_0 = 14.3404$. Furthermore, this new design shows a stiffer response than the first optimisation problem, see Fig. 2a. Additionally the lower overall damage accumulation is visible as the slope of the curve is non-negative compared to the initial design. However, the initial design still shows an overall stiffer structural response than both optima. But since the stiffness is not the objective of this optimisation problem, this is not directly taken into account and would be the subject of e.g. compliance minimisation. Nonetheless, the overall results show that damage optimisation always have to take damage constraints into account in order to circumvent minimisation induced damage localisation.

3.2 Material sensitivity study

In [1], an extended parameter identification of the underlying material model has been conducted. The introduced sensitivity analysis enables additional insight into the problem by studying the derived gradients. The boundary value problem of a plate with a hole with loading and unloading from [1] is chosen as the underlying problem to analyse the response sensitivities of the reaction forces. To calculate these sensitivities, the total variation of the residual vector is applied at the Dirichlet bounded area b, i.e.

$$\delta \mathbf{F}^{\mathrm{ext}} = \left[\mathbf{K}_{ba}\mathbf{S}_a + \mathbf{P}_b + \mathbf{H}_b\,\mathbf{Z}_n\right]\delta \mathbf{m}_p. \tag{23}$$

The list of all material parameters reads $\boldsymbol{m}_{\mathrm{p}} = [E, \nu; \sigma_{\mathrm{y0}}, h, n_{\mathrm{p}}; \eta, \xi_{\mathrm{vol}}, \xi_{\mathrm{iso}}, \xi_{\mathrm{q}}, \xi_{\mathrm{m}}, \eta_{\alpha}, q_{\mathrm{min}}, n_{\mathrm{d}}; c_{\mathrm{d}}, \beta_{\mathrm{d}}]$. It is separated into four blocks divided by semicolons. The first block contains the well-known elastic parameters. The second block is comprised of the three parameters for the plastic evolution. In the third block, all material parameters for the local damage quantification are captured, while the fourth block contains the parameters for the global damage definition of the micro-morphic approach.

The first results are depicted in Fig. 3a. Therein, the response sensitivities of each individual non-elastic material parameter are depicted in each column for each subsequent load step. Analysis of this figure allows to highlight, which material parameter shows the highest sensitivity w.r.t. the reaction forces at each respective load step. The horizontal black lines depict areas, where the simulation is unloaded, with the dotted line as the turning point of those unloading steps. As such, the unloading procedure can be analysed with respect to the response sensitivities. The main problem is the deviance between the dimensions of the material parameters, their impact and as such the response sensitivities. Due to this, the raw data in Fig. 3a cannot be used directly to analyse the gathered information. As such, the first approach is to normalise each respective column, i.e.

$$\delta_{m_i}\mathbf{F}^{\mathrm{ext,norm}} = \frac{\delta_{m_i}\mathbf{F}^{\mathrm{ext}}}{\max\left(\left|\delta_{m_i}\mathbf{F}^{\mathrm{ext}}\right|\right)}. \tag{24}$$

This allows the analysis of the respective parameters on the simulation. However, this no longer allows direct comparison between the material parameters, since the qualitative values are no longer part of the visualised data. The normalised results are depicted in Fig. 3b. Nonetheless, certain aspects can be identified. As such, the yield stress σ_{y0} shows the highest sensitivity at the point of plastic yielding, i.e. step 7 in Fig. 3, which is expected. Additionally, due to plastic yielding and the evolution of damage, the sensitivity of this material parameter decreases with increased load, which is expected, too. Contrary, the hardening modulus h is more sensitive as the simulation progresses due to increased plastic hardening. Focusing on the material parameter q_{min}, which governs the onset of damage evolution, it shows inverse behaviour when compared to the yield stress within the plastic evolution. As such, the sensitivities increase with increasing damage. This is mainly due to the definition of the damage potential and therein the multiplicative dependency of this parameter with respect to the damage

variable, wherein the yield stress is not coupled multiplicative to the hardening variable. Furthermore, the regularisation parameter c_d shows increasing impact with evolving damage, and as such the impact the regularisation has on the observed structural response. Further work is required to make use of this sensitivity data and to allow comparison between the material parameters.

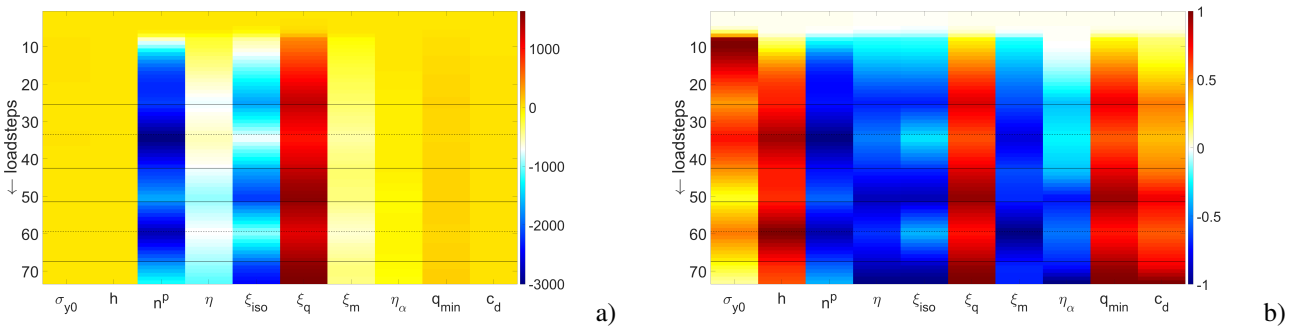

Fig. 3: Sensitivities of the simulated external forces for each non-elastic material parameter. Image a) shows the raw data, while in image b) each column is normalised by its respective maximum absolute value. The black lines represent regions within the simulation where the specimen is unloaded, wherein the dotted lines represent the points at which unloading is reversed again.

4 Summary and outlook

In this work, the sensitivities for an elasto-plastic damage model with a non-local damage regularisation have been derived. By utilising a variational approach, the framework allows for an efficient simultaneous computation of structural and sensitivity responses. The derived gradients have been evaluated either for geometric parameters or for material parameters. In a first example, gradient-based optimisation has been utilised to generate damage resistant geometries within shape optimisation. The results have shown the importance of including damage constraint within the optimisation to ensure geometries, which prevent early damage localisation due the optimisation solution.

In a second example, utilising the gradients for the material parameters, the analysis of the material response sensitivities has been performed. Instead of applying parameter identification, the sensitivities have been analysed directly to visualise their impact within the loading and unloading procedure. Due to their large deviation in their respective dimension, each value has been normalised column-wise, i.e. the sensitivity of each parameter was divided by the absolute maximum value of the sensitivity of each respective parameter. As such, the impact of each parameter on the loading and unloading procedure has been analysed and compared.

Based on this work, additional objective functions can be used for damage optimisation. For example the compliance of the structure can be directly optimised and compared to elastic and elasto-plastic cases. On the basis of the material response sensitivities the work is to be expanded to improve the visualisation of the results as well as the the mapping. The current results only hold information with respect to each separate parameter, but show no overall impact on the material response due to the respective normalisation chosen and allows no direct comparison between each individual parameter. Therefore, a mapping of the material space may be of interest in order to be able to compare the sensitivities of all parameters among each other.

Acknowledgements The financial support of the Deutsche Forschungsgemeinschaft (DFG, German Research Foundation) for project C05 within the Collaborative Research Centre TRR 188 — Projektnummer 278868966 “Damage Controlled Forming Processes” is gratefully acknowledged. Open access funding enabled and organized by Projekt DEAL.

References

[1] L. Sprave and A. Menzel, Acta Mech **231**, 5159-5192 (2020).
[2] Liebe, T., Steinmann, P., and Benallal, Comp. Meth. in Appl. Mech. and Eng. **190**, 6555-6576 (2001).
[3] F. Guhr, L. Sprave, F.-J. Barthold, and A. Menzel, Comp. Mech. **65**, 1105-1124 (2020).
[4] F. Guhr and F.-J. Barthold, Proc. Appl. Math. and Mech. **21**, e202100198 (2021).
[5] J. Liedmann, S. Gerke, F.-J. Barthold, and M. Brünig, Comp. Mech. **66**, 1275-1291 (2020).
[6] J. Liedmann and F.-J. Barthold, Struct. Multidisc. Optim. **61**, 2237–2251 (2020).
[7] F.-J. Barthold, Habilitation, Braunschweiger Schriften zur Mechanik 44-2002, TU Braunschweig (2002).
[8] W. Kijanski, Dissertation, TU Dortmund (2018)
[9] E. A. de Souza Neto, D. R. J. Owen, and D. Peric. Computational Methods for Plasticity (Wiley Chichester, 2008).

